Deciphering the Molecular Mechanisms of BPTF Interactions with Nucleosomes via Molecular Simulations

Ryan Hebert[†,¶] and Jeff Wereszczynski[*,‡,¶]

†*Department of Physics, Illinois Institute of Technology, Chicago, USA*

‡*Departments of Physics and Biology, Illinois Institute of Technology, Chicago, USA*

¶*Center for Molecular Study of Condensed Soft Matter, Illinois Institute of Technology, Chicago, USA*

E-mail: jwereszc@iit.edu

Abstract

Many transcription factors regulate DNA accessibility and gene expression by recognizing post-translational modifications on histone tails within nucleosomes. These interactions are often studied *in vitro* using short peptide mimics of histone tails, which may overlook conformational changes that occur in the full nucleosomal context. Here, we employ molecular dynamics simulations to investigate the binding dynamics of the PHD finger and bromodomain of BPTF, both in solution and bound to either a histone H3 peptide or a full nucleosome. Our results show that BPTF adopts distinct conformational states depending on its binding context, with nucleosome-bound BPTF exhibiting altered histone core interactions. Electrostatic repulsion limits direct reader-

DNA contacts, while histone-DNA hydrogen bonding decreases, suggesting a shift in nucleosome stability. Our findings indicate that BPTF binding to nucleosomes alters local chromatin architecture, potentially contributing to nucleosome remodeling and gene regulation.

1 Introduction

DNA compaction is crucial for fitting eukaryotic DNA within the cell nucleus.[1] DNA in the human genome reaches lengths of approximately 2 m which must be compacted into a nucleus of diameter approximately 5 to 20 µm across.[2,3] DNA is a highly electronegative polymer, with each base pair carrying an electronegative charge in the phosphate backbone. Organization of DNA into chromatin *in vivo* thus requires interactions with a large number of cationic ions and proteins to neutralize this charge.[4] The first step in eukaryotic DNA compaction is the formation of complexes with eight histone proteins.[5,6] Approximately 147 base pairs of DNA wrap around a disk formed of an $(H3/H4)_2$ tetramer and two H2A/H2B dimers to form the nucleosome core particle (NCP).[7] Connecting each NCP are 10 to 90 base pairs of linker DNA, and groups of connected NCPs are joined into chromatin fibers.[6,8] The specific arrangement of nucleosomes within the fiber and thus its diameter vary, with zigzag and solenoid arrangements each observed.[9] On a scale of hundreds of millions of DNA base pairs, the chromatin fibers construct chromosomal territories and chromosomes.[10]

One effect of this multilevel organization of DNA compaction is to modulate the accessibility of the genome for transcription.[11] The formation of nucleosomes and chromatin is known to decrease transcriptional activity by blocking the initiation of RNA polymerase II,[12,13] and for eukaryotic organisms, transcription factors are required for a promoter region to become active.[14] DNA-binding transcription factors must also compete with histones for DNA binding affinity,[15–17] but a subset of eukaryotic transcription factors feature reader domains

which recognize post-translational modifications (PTMs) of histone proteins.[18,19]

Histones are composed of disordered N-terminus "tails" and bundles of three alpha helices connected by two loops.[20–22] Strong electrostatic interactions between phosphates, lysines, and arginines create an interface between the helices and turns of the histone cores with DNA, compacting the negatively charged DNA and the positively charged histones.[23,24] The histone tails contain about 25% of the total histone mass and are also rich in lysine and arginine, leading to a similar strong DNA association on the exterior of the NCP.[25,26] Along these tails are many sites for PTMs, among the most common being lysine acetylation and lysine methylation.[27] PTMs on histones are also markers of active transcriptional sites, such that the histone code is hypothesized to be determinative of gene expression along with the genetic code.[18,28] Part of the mechanism lies in the altered charge of the amino acids to which PTMs are applied, decreasing the strength of the DNA-histone tail association and increasing the likelihood that a reader may bind to the tail.[29] However, NMR experiments and molecular dynamics (MD) simulations show that histone tails associate preferentially with DNA in the NCP to the exclusion of PTM readers in mononucleosomes.[30,31] Histone tails are subject to intermolecular forces in chromatin that are absent in mononucleosome systems, which may free them for interactions with reader domains.[32]

One common reader domain motif is the plant homeodomain (PHD) finger, featuring a three sided cage that recognizes PTMs and zinc binding domains.[33,34] PHD fingers are found in more than 100 human proteins, often accompanied by other chromatin binding domains, and most commonly bind to lysine 4 on histone H3 in various methylation and acetylation states.[35,36] A bromodomain is another reader with its own acetylated lysine binding pocket and features four parallel alpha helices connected by loop or loop-helix-loop regions.[37,38] Bromodomain PHD Finger Transcription Factor (BPTF) is an example of a protein containing both domains - A PHD finger recognizing trimethylated lysine 4 on H3 (H3K4me3) and

a bromodomain recognizing acetylated lysine 16 on H4 (H4K16ac).[33,39] H3K4me3 notably marks the beginning of many transcription sites in the genome,[40–42] making it an important PTM for structural studies of reader domains. BPTF is part of the Nucleosome Remodeling Factor in humans (hNURF), known to be involved in neuronal development[43,44] and catalyzing nucleosome sliding.[45,46] The other components of hNURF are SNF2L and pRBAP46/48, an ATPase and a histone binding domain, respectively.[43] Studies have focused on BPTF as a target for drug therapy due to its enhancement of cancerous tissue growth[39,47–49] in addition to its contribution as part of hNURF in chromatin remodeling.

BPTF reader domains are typically studied *in vitro* using short peptides that mimic the histone tail and PTM,[33,50] which may preclude understanding of the dynamics in the context of full-length nucleosomes and chromatin. Observation of such systems *in vivo* and production of full NCP-reader systems *in vitro* likewise proves difficult.[51] Here, we have used classical molecular dynamics (MD) simulations to explore the differences in the motions and interactions of a PHD finger and finger-linker-bromodomain fragment of BPTF in solution, with a peptide fragment mimicking H3, and a full-length NCP. MD simulations provide an ideal computational counterpart to *in vitro* experiments, as they can provide atomistic details of nucleosome motions across a wide range of length and timescales in nucleosome systems.[52–57] Our findings indicate that NCP binding of the BPTF fragment results in different conformation states of the reader protein that are not accounted for when binding to H3-mimicking peptides, as well as a reduction in histone-DNA hydrogen bonding resulting from increased histone fluctuations when binding to PHD fingers. This suggests a potential mechanism to induce nucleosome sliding shared by PHD finger containing proteins, and that the full dynamics of readers may not be fully captured in studies with short peptides.

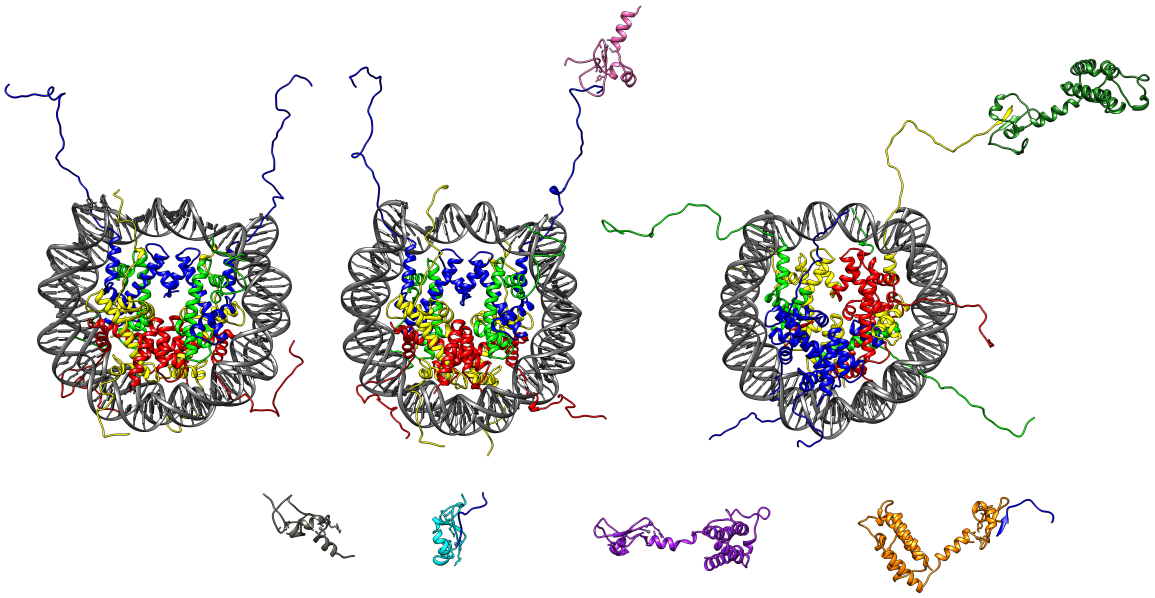

Figure 1: Top left through top right: Sample frames from early in the simulations for the nucleosome core particle, the NCP with bound PHD finger, and the NCP with bound BPTF fragment. Bottom left through bottom right: Sample frames from early in the simulations for the PHD finger, PHD finger with short peptide, BPTF fragment, and BPTF fragment with short peptide.

2 Methods

2.1 System construction

NCP models were generated by taking the 1KX5 crystal structure,[7] remodeling the H3 tails to extend away from the NCP core using UCSF Chimera's Modeller interface,[58,59] and introducing a trimethylation to lysine 4 on one of the H3 tails using tleap from the AmberTools suite.[60] PHD finger and BPTF models were from the 2F6J crystal structure,[33] using chain A for BPTF and the chain P H3 residues. Using UCSF Chimera's Modeller interface,[58,59] residues 1-15 of H3 were remodeled in reader with peptide systems from the six resolved residues in chain P of the 2F6J structure. PHD finger systems were modified from BPTF by removing the bromodomain and loop region after the helical linker beyond residue 61. NCP and reader complexes were created by using the alignment tools in Chimera to align H3 1-6, deleting those residues from the NCP, and splicing the residues from the 2F6J structure in their place. This maintained the H3 binding mode to the PHD finger and the histone core positioning in the NCP. All starting structures are represented in Figure 1.

Solvation and generation of parameter and starting coordinate files was performed in tleap and parmed from AmberTools.[60] All simulations used the ff19SB force field,[61] an additional library for trimethylated lysine,[62] OPC water model,[63] and Li and Merz 12-6 OPC water ions.[64,65] NCP simulations also used the BSC1 DNA force field.[66] The BPTF PHD finger contains two zinc metal centers which were paramaterized with the Zinc Amber Force Field.[67] All but two systems were solvated in water boxes with a 10 Å buffer, neutralized with Na+ ions, and additional Na+ and Cl- ions added to give final ion concentrations of 150 mM NaCl. To prevent self-image interactions, BPTF systems without nucleosomes were solvated in isometric water boxes with the same ion neutralization and final ion concentrations. To

decrease computation time, hydrogen mass repartitioning[68] was employed in parmed, changing the masses of all non-solvent hydrogens to three AMUs and compensating by reducing the mass of the attached heavy atom.

2.2 Molecular dynamics simulations

Systems were minimized twice for 10000 steps, swapping from steepest descent to conjugate gradient after 5000 steps. The first minimization applied a $10\,\mathrm{kcal/mol\,Å^{-2}}$ harmonic restraint to all heavy atoms and the second minimization had no restraints. Structures were then heated from 5 to 300 K over 5 ps using a Berendsen barostat and Langevin dynamics in an NVT ensemble[69,70] with $10\,\mathrm{kcal/mol\,Å^{-2}}$ harmonic restraints on solute heavy atoms. These restraints were then relaxed by factors of 1/3 every 100 ps in the NPT ensemble and completely removed after 600 ps. All systems after relaxation were simulated in five copies each using pmemd.cuda[60,71–73] for an additional microsecond in the NPT ensemble at 300 K, 4 fs timesteps, and a 10 Å non-bonded cutoff using local resources and resources provided by the Extreme Science and Engineering Discovery Environment (XSEDE).[74] Based on root mean square deviation from the first frame (RMSD) data calculated using cpptraj[60] and observing H3 tail collapse in each trajectory, the first 300 nanoseconds of each simulation are considered equilibration time in analyses. All minimization, heating, relaxation, and simulations were performed using Amber 20.[60]

2.3 Simulation Analyses

RMSD, angle measurements between the PHD finger and bromodomain, root mean squared fluctuations (RMSF), hydrogen bonds, and radius of gyration analyses were performed using cpptraj from AmberTools20[60] on post-equilibration trajectory frames. Angles were measured using vector dot products - one vector connected the centers of mass of α-carbons 7 - 48 in

the PHD finger to α-carbons 49 - 56 in the linker, and the second vector connected the centers of mass of α-carbons 137 - 142 and 148 - 153 near the bromodomain binding pocket to centers of mass of α-carbons 125 - 130 and 160 - 165 (see Figure S1).

PHD finger binding pocket volumes were calculated using the sphere method in the Epock plugin for VMD.[75,76] Trajectories were stripped of all but the PHD finger and aligned to residues 6 - 50 of the H3 peptide bound PHD finger from the 2F6J structure in VMD. 5.0 Å inclusion spheres were centered on the first five H3 peptide residues in the binding pocket.

To measure the RMSFs, histones first underwent an RMSD alignment to the heavy atoms in their alpha helices on the first post-equilibration frame. The average atomic positions of the histone heavy atoms was then computed, and RMSFs were then measured referencing these average positions. RMSFs of the PHD finger and bromodomain was measured in a similar manner, aligning to the heavy atoms in the first 59 residues in the PHD finger and last 104 residues in the BPTF fragment for the bromodomain. Hydrogen bonds were calculated using a donor-acceptor cutoff of 3.0 Å and a cutoff angle of 135°. All intramolecular and DNA base pair hydrogen bonds were excluded. Normalized mutual information scores of NCP systems were taken using CorrelationPlus.[77] Solvent accessible surface area was calculated in AmberTools using the linear combinations of pairwise overlaps method[78] on the H3 tails.

Per-residue H3 contacts with DNA and readers, histone and DNA contacts, and measurement of reader atoms within a Debye length of DNA were calculated using MDAnalysis[79,80] with 4.0 Å cutoffs between heavy atoms for contacts and 7.8 Å cutoffs for the Debye length in 150 mM neutral NaCl.[81] Contacts across adjacent residues were considered correlated in reporting averages across the H3 tail. Histone and DNA contacts were calculated in a similar manner, where residues 1 - 16 in H2A, 1 - 34 in H2B, 1 - 36 in H3, and 1 - 30 in H4 are

considered tails. The remaining residues were considered to be the histone core.

MMGBSA[82] results were calculated using MMPBSA.py[83] in Amber20,[60] using the reader trajectories as the receptor, NCP trajectories as ligand, and reader-NCP trajectories as complexes for inputs. All post-equilibration frames of ligand and receptor trajectories were used in each GBSA analysis, and complex trajectories were run one trajectory at a time with an igb value of 8, corresponding to mbondi3 radii.[84,85] The timeseries tool of the Python implementation of the multistate Bennett acceptance ratio (pymbar)[86,87] was used to account for statistical inefficiencies in evaluating energetics from individual simulations. Final results presented here are average values.

3 Results

3.1 BPTF is dynamically affected by the nucleosome context

An array of molecular models were constructed to examine the effects of binding of the BPTF PHD finger and the bromodomain to full-length nucleosomes. These included models of an isolated PHD finger and an isolated PHD-linker-bromodomain complex, models of a PHD finger and a PHD-linker-bromodomain complex bound to an H3 peptide, models of a PHD finger and a PHD-linker-bromodomain complex bound to a full-length nucleosome, and an isolated nucleosome system (Figure 1). Each system was simulated five times for 1.0 µs, for a total of 35.0 µs of simulation (Table 1).

Regardless of whether it was free, peptide, or nucleosome bound, simulations of the PHD-linker-bromodomain (hereafter referred to as BPTF) showed a wide range of conformational flexibility between the PHD finger and bromodomain. In each simulation, the individual PHD and bromodomain domains were relatively stable, with RMSD values ranging from 1.4-7.2 Å and 1.3-4.9 Å for the PHD finger and bromodomain respectively (Figure S2).

Table 1: A summary of the simulation sampling time of each system.

System	Simulation Time (ns)	Replicates	Total (ns)
PHD Finger (PHD)	1000	5	5000
PHD + Peptide	1000	5	5000
BPTF fragment (BPTF)	1000	5	5000
BPTF + Peptide	1000	5	5000
H3K4me3 Nucleosome (NCP)	1000	5	5000
PHD + NCP	1000	5	5000
BPTF + NCP	1000	5	5000
		Total Simulation Time:	35000

However, when the RMSD of the entire BPTF complex was measured, there was an increase in the overall RMSD to as high as 15.0 Å. To further characterize this flexibility, we measured the angle between the PHD finger and the bromodomain in BPTF. An angle of 0° indicates a fully closed state where the bromodomain has folded onto the PHD finger, while an angle of 180° indicates a fully open state. This angle ranged from 43.8-180.0 ° for BPTF in solution, 30.6-179.7° when bound to the peptide and 7.1-179.8 ° when bound to the NCP (Figure 2). Large swings of over 100° are seen in time series data in all systems (Figure S1). This indicates that BPTF takes a large variety of conformation states based on the relative orientation of the bromodomain to the PHD finger. It also indicates that NCP binding led to a larger sampling of more compact, closed states. This flexibility is a close match to the radius of gyration, which ranged from 17.5-29.1 Å, with the mode of conformations at 25.0 Å in the unbound, 23.8 Å in the peptide-bound, and 21.9 Å NCP-bound states (Figure S3). The variation indicates a key difference in the motions of BPTF in the full-length NCP compared to the unbound or more restricted peptide-bound systems. NCP-bound BPTF demonstrates greater sampling of more compact conformations and a more even spread between compact and open conformations. In general, however, every BPTF system demonstrated a large degree of flexibility.

Binding states also affect the volume of the PHD finger's binding pocket. Using Epock,[76] we estimated the volume of the H3 binding pocket of the PHD finger. When free in solution,

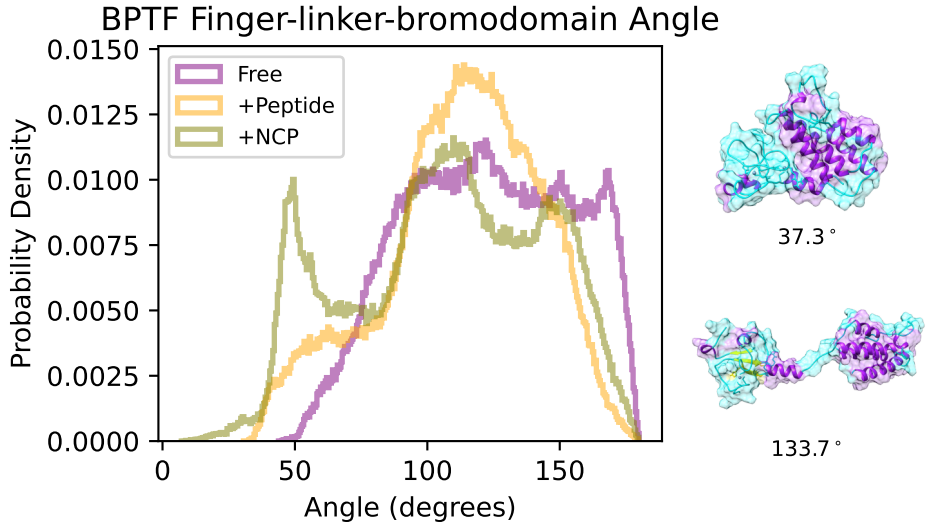

Figure 2: The angle between the bromodomain and the PHD finger-linker axis shows flexibility in the BPTF fragment as the linker between the PHD finger and bromodomain acts as a hinge. H3 binding increases sampling of more compact conformations, with even larger sampling of compact conformations in NCP bound systems. Two sample conformations show the large scale motions of the bromodomain relative to the PHD finger.

the volume was 1331.0±51.9 Å^3 in the PHD finger system and 1279.8± 54.1Å^3 in the BPTF system. When bound to the H3 fragment, the mean pocket volumes increased significantly to 1423.7±18.4 Å^3 and 1423.8±19.7 Å^3 for the PHD finger and BPTF, compared to 1452.3±25.5 Å^3 and 1457.9±19.4 Å^3 respectively when NCP bound (Figure 3). This increase in volume also corresponded to a decrease in the flexibility of the binding site, measured by the RMSF of the Cα atoms in the binding pocket region (residues 17-48, Figure 4). In both the PHD finger and the BPTF systems, there was a decrease in RMSFs of ∼0.4-0.5 Å throughout this region. NCP bound PHD fingers and BPTF saw smaller average decreases of ∼0.2-0.3 Å in the same region. This is also seen over time as unbound readers exhibit larger fluctuations in the binding pocket volume than bound readers (Figure S4). Together, these results suggest that H3 binding stabilizes the PHD finger and keeps the binding pocket open in systems bound to peptides and NCPs, and that this effect is slightly amplified in NCP systems.

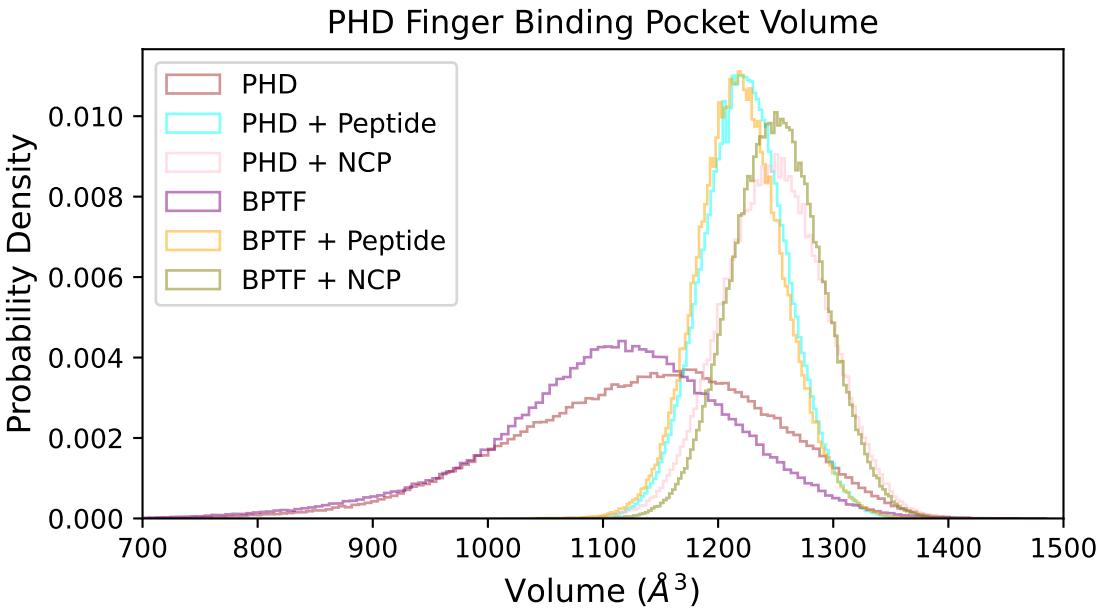

Figure 3: Measurement of the binding pocket volume of the PHD finger in all systems. By specifying points centered on residues, cylinders are placed to encompass the binding pocket. Gridpoints are generated within these cylinders and without overlapping the protein surface to calculate the volume. Aligning the trajectory allows a dynamic tracking of the pocket volume. H3 binding keeps the pocket open, and nucleosome proximity appears to augment this effect.

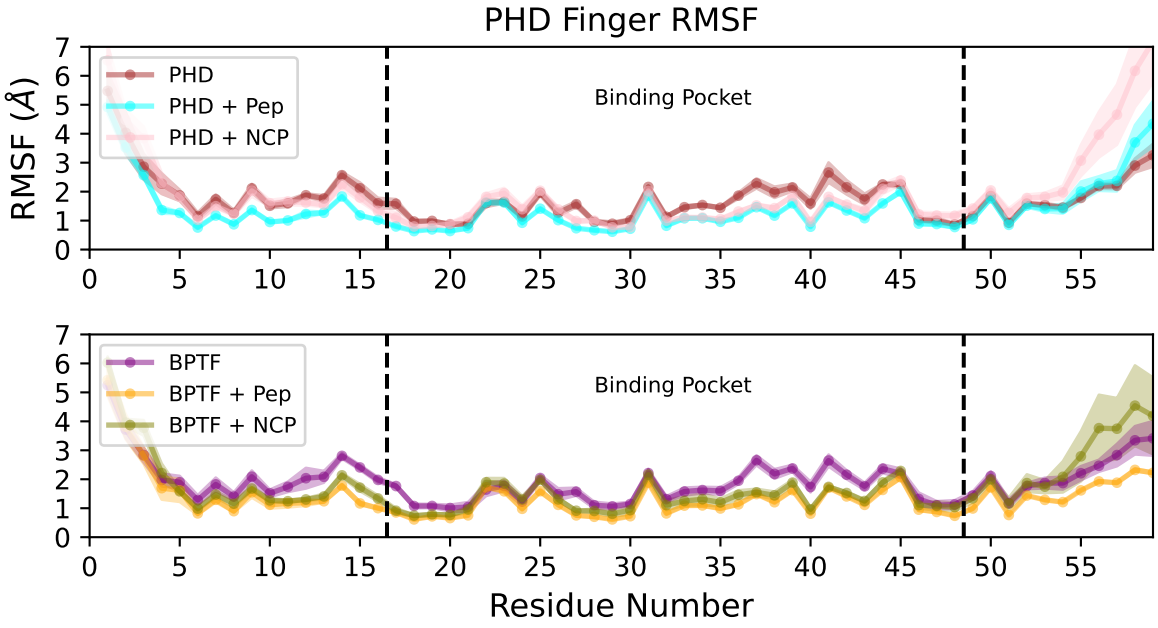

Figure 4: Top: Root mean square fluctuations of the first 59 PHD finger residues from all systems. H3 binding stabilizes the binding pocket region, with a smaller effect on the full-length nucleosome.

3.2 The PHD finger competes with DNA for H3 tail association

In all cases, NCP H3 tails started their simulations extended and were allowed to collapse onto the core. The PHD finger crystal structure included the first six residues of the histone tail in the binding pocket, and these residues maintained their association with the PHD finger to the exclusion of DNA. H3A1-H3T6 made approximately 319±22 and 308±39 contacts on average with the PHD finger with and without the bromodomain, respectively. These numbers were relatively consistent with the systems run without full NCPs, 333±14 and 330±15 contacts with and without a bromodomain. This dropped off quickly to less than 10 for all subsequent tail residues in NCP systems and all residues after A7 in systems lacking NCPs. In contrast, these residues in unbound NCP systems had 107±35 contacts with DNA vs. 3±6 and 7±7 for PHD and BPTF bound systems, respectively (Figure S5). Overall, the

first 15 H3 tail residues in NCP systems without readers had 166±43 solute contacts, and H3 tail residues bound to readers without the NCP had 363±20 and 364±18 solute contacts with and without the bromodomain. Residues 7 through 15 contacted DNA more similarly to systems without readers, leading to total solute contacts across the first 15 residues of 379±37 and 453±55 contacts with and without the bromodomain (Figure 5). This indicates that the first six residues maintain preferential binding to the reader to the exclusion of DNA, while residues 7 through 15 had more contacts in PHD bound systems. From this we conclude that binding to a reader reduces H3-DNA tail association, and that binding to a more dynamic reader like BPTF has a larger reduction in H3-DNA association.

The bound PHD finger and BPTF made minimal to no contact with DNA. Instead, the PHD finger maintained consistent contact with H3 which in turn formed a buffer between the transcription factor and DNA. We also observed a reduction in reader-bound systems of the solvent accessible surface area of the modified H3 tail (Figure S6), indicating the tail had more solute interactions in reader systems than unbound NCP systems. These factors led us to use MMGBSA analysis[82] to estimate the driving interactions of the reader association. Both systems showed a large electrostatic repulsion, with the PHD systems having an estimated 201.9 ± 8.7 $\frac{kcal}{mol}$ and BPTF 156.9 ± 10.0 $\frac{kcal}{mol}$ difference in electrostatic energy. This was coupled with significant but smaller unfavorable internal energies of 27.9 ± 3.5 and 32.4 ± 3.8 $\frac{kcal}{mol}$, respectively, indicating unfavorable bond angles. There was an overall net negative energy due to highly favorable Van der Waals interactions of -349.1 ± 9.1 and -344.9 ± 10.2 $\frac{kcal}{mol}$ (Table 2). The PHD finger and BPTF carry net negative charges, and came within a Debye length of the negatively charged DNA for much of the post-equilibration frames (see Figure S7), indicating the two were within range of each other's electrostatic influence in solution. From this, we conclude that electrostatic repulsion between the negatively charged PHD finger and DNA leads to a lack of contacts, and that PHD binding with H3 is sufficiently strong to prevent disassociation of the reader. The nature

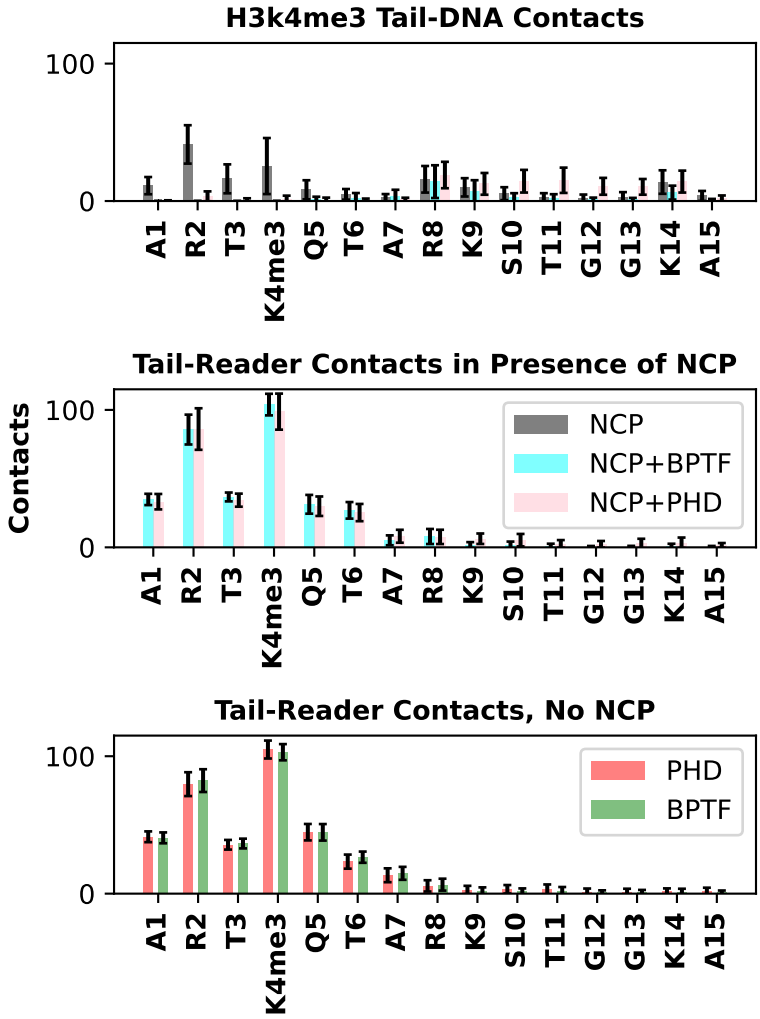

	DNA Contacts	Reader Contacts	Total
NCP	166 ± 43	--	166 ± 43
PHD + Peptide	--	363 ± 20	363 ± 20
NCP + PHD	106 ± 32	347 ± 46	453 ± 55
BPTF + Peptide	--	364 ± 18	364 ± 18
NCP + BPTF	41 ± 30	338 ± 25	379 ± 37

Figure 5: The distribution of contacts over the first 15 residues of the modified H3 tail. Top: Tail contacts with DNA in all NCP systems. Top Middle: Tail contacts with the reader protein in NCP systems. Bottom middle: Tail contacts with the reader protein without the NCP. Bottom: A table summarizing the split in contacts between the reader and DNA. The readers compete with DNA for tail association, with more tail contacts with the reader at the binding pocket and less along the tail. H3 1-15 contacts with the readers shows strong consistency with and without the full NCP.

of GBSA analyses should encourage caution in trusting the precision of these numbers, and we instead emphasize their relative magnitudes to conclude that Van der Waals interactions stabilized the association of the PHD finger with the full-length NCP.

Table 2: Three trajectory GBSA results for the NCP + Reader systems in kcal/mol. Van der Waals interactions drive the stability of the association between the nucleosome core and reader domains.

System	ΔE_{elec}	$\Delta E_{internal}$	ΔE_{VdW}	ΔE_{total}
PHD + NCP	201.9 ± 8.7	27.9 ± 3.5	-349.1 ± 9.1	-119.2 ± 13.1
BPTF + NCP	156.9 ± 10.0	32.4 ± 3.8	-344.9 ± 10.2	-155.6 ± 14.8

Bound preferably to the PHD finger, the histone H3 tail experiences a reduction in stability downstream of the PHD binding site. RMSFs of the H3 tail reveal much increased variation in bound systems, with BPTF bound systems seeing the largest variance. The first 23 H3 residues saw an average RMSF of 6.4 ± 2.5 Å from average structures, vs. 9.4 ± 5.1 Å and 10.4 ± 27.2 Å in PHD and BPTF bound systems, respectively (Figure 6). This, along with the lack of reader-DNA contacts and reduction in H3-DNA contacts, indicates that binding to readers results in more mobile, less restricted H3 tails. This increased tail mobility also propagates into the histone core.

3.3 The reader domains affect histone - DNA association

In addition to increased histone tail fluctuations, reader binding also increased fluctuations of core H3. Residues P43-Q55 in H3 had RMSFs on average of 1.1 ± 0.0 Å for unbound NCPs, 2.1 ± 0.5 Å for PHD bound NCPs, and 3.7 ± 2.1 Å for BPTF bound NCPs. Adjacent H3, which was not bound to a reader, saw averages of 1.0 ± 0.0, 1.3 ± 0.1, and 2.7 ± 1.2 Å respectively from unbound, PHD bound, and BPTF bound systems (Figure 6). Similar differences were observed in the fluctuation of other histones in the octamer bundle (Figures S8, S9, and S10). We performed a mutual information analysis of the NCP in each system, and observed a notably large reduction in the correlation of the H3 histone tail bound to

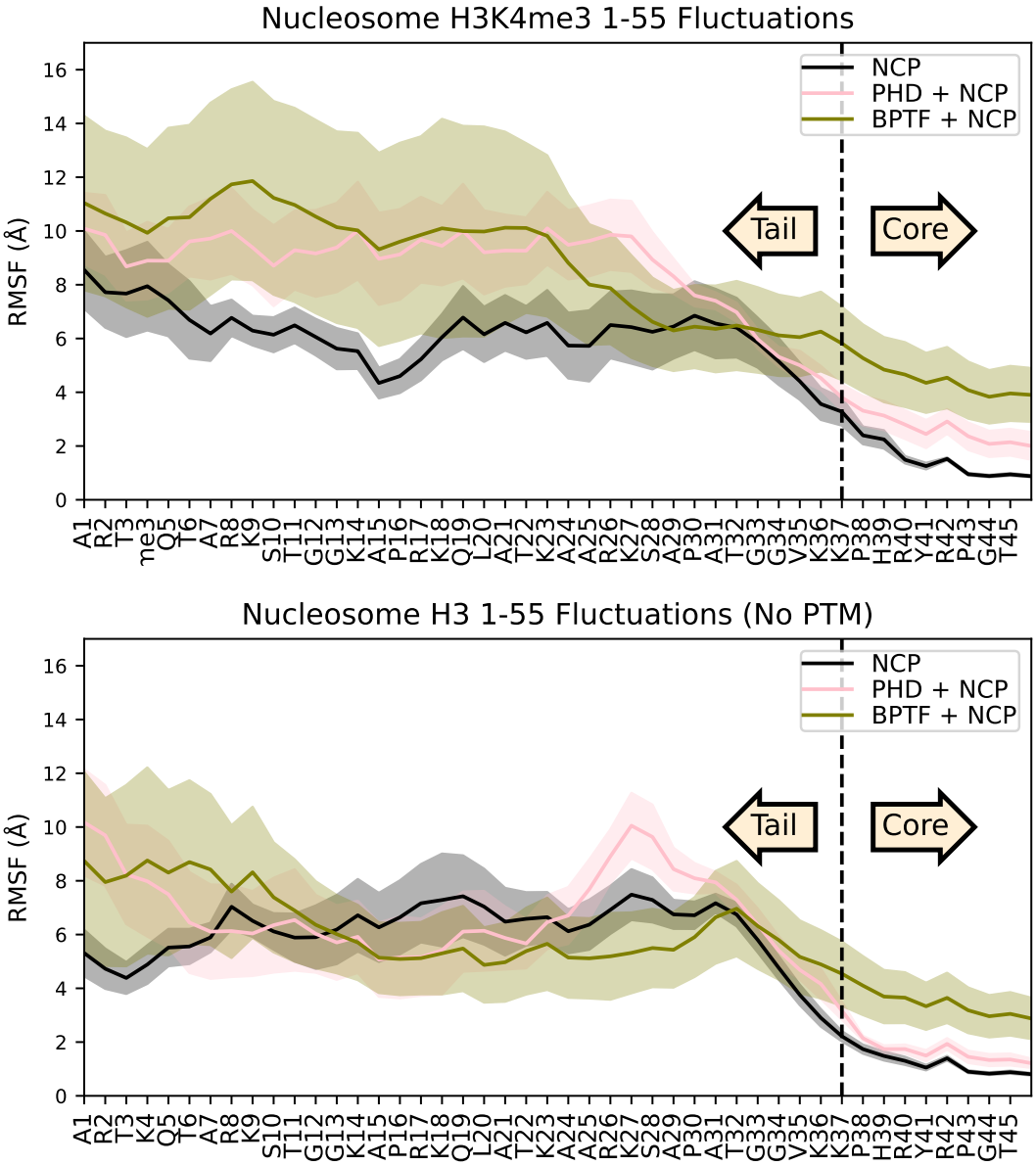

Figure 6: Fluctuations of both histones H3 in each system. In all cases, alignment is to the helices in the H3 core. Top: Fluctuations by residue in the modified H3K4me3 system, where the readers were bound. Trimethylation of lysine 4 and reader domain binding results in an increase in the fluctuations of core H3. Bottom: Fluctuations by residue of the mirror histone H3, where the readers are not bound and there is no PTM. Fluctuation increases from reader binding also extend into the other core histones.

BPTF. The histone core in this system had a smaller but still noticeable increase in core correlations, where PHD bound systems appear to have less pronounced differences from

unbound NCP systems (Figure S11). This suggests that BPTF binding not only reduces DNA interactions, but that the corresponding fluctuations in H3 affect the entire protein and, through allosteric interactions, the entire histone core.

These increased core motions also corresponded with a shift in the association of the histones with DNA. The difference in total contacts between histones and DNA was less than 2% between the readerless and reader-bound systems, despite the corresponding 7% and 8% losses in H3 contacts in the PHD-bound and BPTF-bound systems, respectively. On average, NCP systems without readers had 9070±1290 H3 tail contacts compared to 6346±1232 and 5933±1192 in PHD and BPTF bound systems, while the core had 53018±1765 compared to 51417±1752 and 51306±1569 contacts. These losses correspond with increased H4 tail contacts of 2946±1332 in PHD and 2215±1231 in BPTF bound NCP systems, with negligible changes in core H4. H2A also appeared to have increased contacts, although these differences were within the margin of error. These results indicate a shift in the distribution of contacts with DNA as a result of binding to the reader (Figure 7).

Corresponding to this shift in contacts was a loss of hydrogen bonds between histones and DNA. On average, both H3 proteins made a total of 49±3 hydrogen bonds in the NCP system with no readers, versus 37±4 in both systems with readers. This was split between the histone tail and the core, with the modified tail having 6±1 and the unmodified having 9±1 hydrogen bonds with DNA with no readers. The hydrogen bonds dropped to 4±1 in the modified tail and 6±1 in the unmodified tail in PHD bound systems, and 3±1 and 7±1 in BPTF bound systems. Given that the H3 tail of one H3 histone was preferentially bound to a PHD finger and the first 30 residues, in general, had less contact with DNA, this was expected. Less expected were the decreases in the other histones; both H4 contributed a total of 26±2 hydrogen bonds with DNA without readers versus 21±3 and 23±2 with readers, with no significant difference in the tails. H2A contributed 31±2 versus 24±4 and 25±3, and

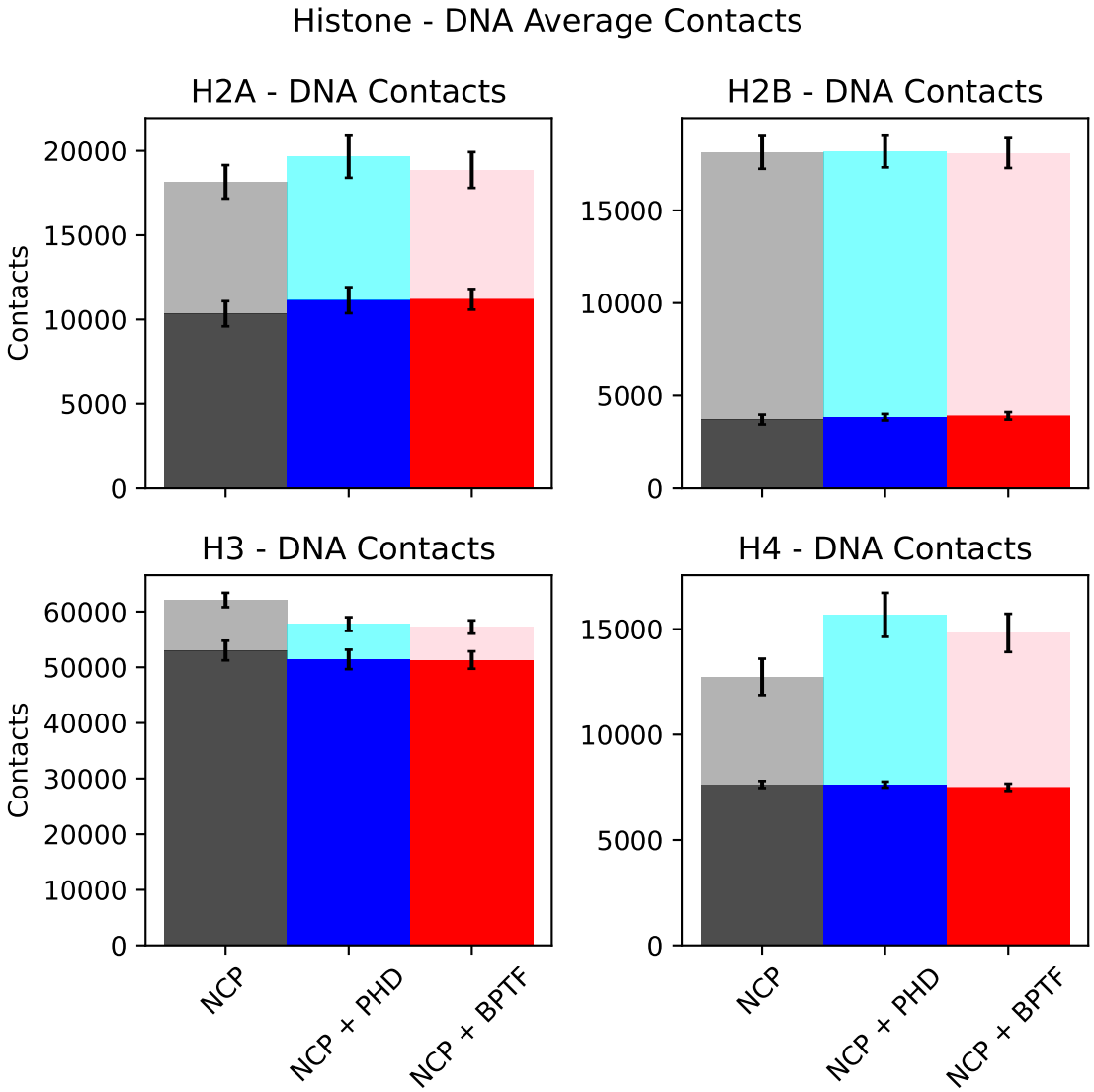

Figure 7: Average atomic contacts between histone tails and histone cores with DNA across the systems with reader domains. Values are stacked with tail contacts on top of core contacts. In both cases histone H3 loses contacts from reader binding, while H2A and H4 gain contacts. Binding BPTF results in a small net loss of H2B-DNA contacts, while PHD binding results in a small net increase. The total number of atomic contacts between histones and DNA in PHD binding systems has a slight net increase, and BPTF binding systems see a net decrease in contacts, indicating a shift in contact distributions.

H2B contributed 30±2 versus 24±3 and 25±3. In total, reader systems saw a reduction of 25 to 29 hydrogen bonds between histones and DNA, a significant reduction in the binding between histone core and DNA (Figure 8). These results indicate that binding to readers may "tug" on the histone, shifting the entire core. Likewise, these shifts and reduction in hydrogen bonding suggest a loosening of DNA and histone association.

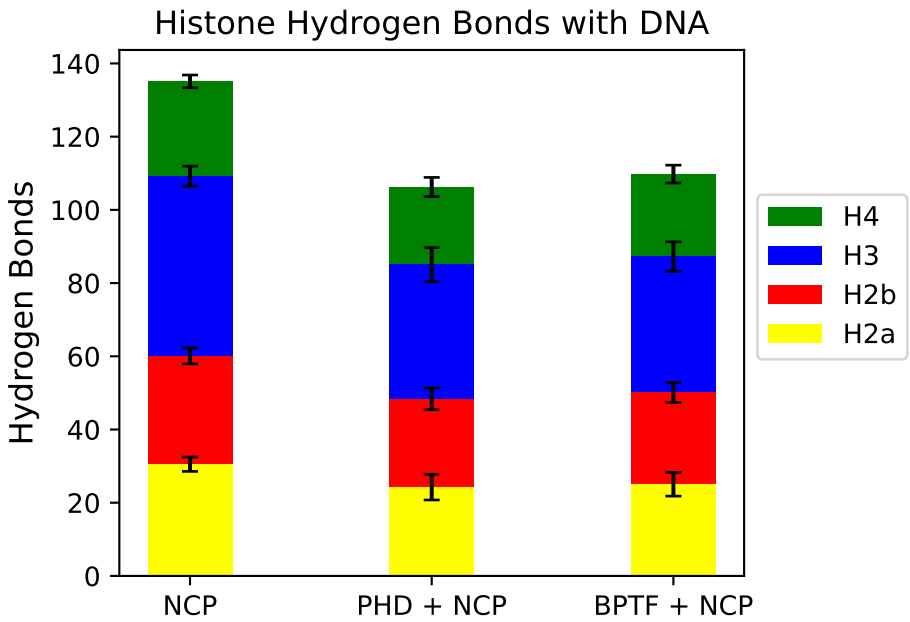

Figure 8: Comparison of the total number of hydrogen bonds between the histones and DNA. This difference is spread across the cores and tails of all of the histones, with both H3 histones constituting a third of this difference despite the PHD finger only being bound to one of them.

4 Discussion

This study used all-atom MD simulations to explore the dynamics of nucleosomes bound to a PTM reader domain. PTMs decrease histone tail association with DNA,[30] which otherwise inhibits association with BPTF's PHD finger in mononucleosomes. Here, we started with the PHD finger already associated with H3K4me3 with the H3 tails in an extended conformation, allowing the tails to collapse in equilibration of the simulation runs. The presence of the H3

1-15 peptide had a consistent stabilizing effect on the BPTF fragment compared to systems without the peptide and on the full-length nucleosome. PHD finger binding pocket volume, RMSF, RMSD, and BPTF radius of gyration (Figures 3, 4, S2, and S3) all indicated there were differences in reader motions bound to the NCP compared to when bound to a short peptide. H3 contacts between the PHD finger and DNA and analysis of the binding affinity (Figure 5 and Table 2) suggest that even when H3 was already stably bound to the PHD finger, DNA competed with the PHD finger for H3 tail association. Trimethylation has no effect on the charge of the attached lysine and on its own should not significantly alter the electrostatic environment.

Despite the close proximity to compete over contacts, the PHD finger maintained minimal, if any, contact with DNA directly while the H3 tail settled between them. In the five runs where the bromodomain was present with the NCP, no contacts were observed between the bromodomain and any other part of the NCP. In all simulations, the bromodomain preferred an orientation toward the solution away from the NCP, and no other tail association with the bromodomain was observed. The consistency of this result suggests an entropic penalty in associating with H4 within the same nucleosome as the associated H3.

PHD fingers interact with other proteins simultaneously with H3.[88,89] The electrostatic interactions observed with DNA, the corresponding increase in the fluctuations of the H3 tail, and the variation in position on the NCP of the collapsed tail-reader complex indicate that the potential interactions of the PHD finger with other proteins may not be limited by DNA binding specificity. PHD fingers which recognize H3K4me3 are motifs of many different proteins with activation, repressor, and remodeling functions,[45,90–93] indicating that the larger protein complex ultimately determines the biological function of PHD binding to H3. Given this, the differences in histone and DNA hydrogen bonding observed between reader bound and unbound NCP systems may indicate a precursor mechanism at the NCP level to facil-

itate remodeling by hNURF. If these differences were a general result of binding by PHD fingers, other proteins in complex with them may reinforce against or cooperate in NCP destabilization and DNA accessibility.

Other finger-linker-bromodomain systems have been observed to have cooperative effects independent of the length of the linker.[91] More compact conformations conducive to direct bromodomain-finger interactions were observed when bound to the full-length NCP compared to the H3 fragment. While we have not observed simultaneous bromodomain and PHD finger binding, freeing the loop region between the helical linker and bromodomain to flex, this does not preclude the possibility that other units of complexes formed with BPTF will restrict the flexibility of the finger-linker-bromodomain subunit. Orienting the bromodomain away from the nucleosome from the beginning may also have reduced the likelihood of direct contact between the two. Our nucleosomes also did not have any H4 acetylation marks, an essential ingredient to bromodomain binding[39] especially in conjunction with H3K4me3 binding of the PHD finger.

No other changes were made to the amino acid and nucleic acid sequences of the original structure beyond the remodeling of the H3 tails. At the sampled time scales, some increased fluctuations in the tail were observed as a result of this trimethylation and the presence of the readers, including increased fluctuations in the core when the bromodomain is present. A known effect of BPTF-containing complexes is the induction of nucleosome sliding, a remodeling feature that occurs on timescales currently inaccessible to conventional all-atom simulations,[94] though may be seen in coarse grained systems.[95] Furthermore, this study was performed on a mononucleosome, but the initial association of the reader with the histone tail likely requires intermolecular forces present *in vivo* but absent in mononucleosome systems.[30,31] Multiple coexisting PTMs are expected to be found within a given histone octamer,[96] with the different combinations leading to many potential cross-talk ef-

fects. Some of these include further H3 tail modifications known to decrease PHD finger binding affinity and H4K16ac, considered BPTF's canonical binding mode.[39] Even so, the increased histone fluctuations and the decreased hydrogen bonding between histones and DNA suggest that even small reader binding may contribute to an increase in instability of the nucleosome core. However, no substantial changes in total DNA contacts or unraveling of DNA were observed. As PHD fingers and finger-bromodomain structures are constituents of complexes that both inhibit and enhance transcription, perhaps the associated increase in histone fluctuations with an unbound bromodomain indicates that larger and dynamic proteins binding to histones facilitate or inhibit transcription through allosteric effects on histone-DNA binding.

5 Data availability

MD trajectories generated in this study are available on Zenodo at: `https://doi.org/10.5281/zenodo.14926478`

References

(1) Estévez-Torres, A.; Baigl, D. DNA compaction: fundamentals and applications. *Soft Matter* **2011**, *7*, 6746–6756.

(2) Piovesan, A.; Pelleri, M. C.; Antonaros, F.; Strippoli, P.; Caracausi, M.; Vitale, L. On the length, weight and GC content of the human genome. *BMC Res Notes* **2019**, *12*, 106.

(3) Lammerding, J. Mechanics of the nucleus. *Comprehensive physiology* **2011**, *1*, 783.

(4) Joyeux, M. Compaction of bacterial genomic DNA: clarifying the concepts. *Journal of Physics: Condensed Matter* **2015**, *27*, 383001.

(5) Emanuel, M.; Radja, N. H.; Henriksson, A.; Schiessel, H. The physics behind the larger scale organization of DNA in eukaryotes. *Phys Biol* **2009**, *6*, 025008.

(6) Tan, S.; Davey, C. A. Nucleosome structural studies. *Curr Opin Struct Biol* **2011**, *21*, 128–136.

(7) Davey, C. A.; Sargent, D. F.; Luger, K.; Maeder, A. W.; Richmond, T. J. Solvent mediated interactions in the structure of the nucleosome core particle at 1.9 a resolution. *J Mol Biol* **2002**, *319*, 1097–1113.

(8) Fransz, P.; De Jong, H. From nucleosome to chromosome: a dynamic organization of genetic information. *The Plant Journal* **2011**, *66*, 4–17.

(9) Aljahani, A.; Mauksch, C.; Oudelaar, A. M. The relationship between nucleosome positioning and higher-order genome folding. *Current Opinion in Cell Biology* **2024**, *89*, 102398.

(10) Tiana, G.; Giorgetti, L. Integrating experiment, theory and simulation to determine the structure and dynamics of mammalian chromosomes. *Current opinion in structural biology* **2018**, *49*, 11–17.

(11) Risca, V. I.; Denny, S. K.; Straight, A. F.; Greenleaf, W. J. Variable chromatin structure revealed by in situ spatially correlated DNA cleavage mapping. *Nature* **2017**, *541*, 237–241.

(12) Laybourn, P. J.; Kadonaga, J. T. Role of nucleosomal cores and histone H1 in regulation of transcription by RNA polymerase II. *Science* **1991**, *254*, 238–245.

(13) Haberle, V.; Stark, A. Eukaryotic core promoters and the functional basis of transcription initiation. *Nature reviews Molecular cell biology* **2018**, *19*, 621–637.

(14) Struhl, K. Fundamentally different logic of gene regulation in eukaryotes and prokaryotes. *Cell* **1999**, *98*, 1–4.

(15) Smith, N. C.; Matthews, J. M. Mechanisms of DNA-binding specificity and functional gene regulation by transcription factors. *Curr Opin Struct Biol* **2016**, *38*, 68–74.

(16) Luzete-Monteiro, E.; Zaret, K. S. Structures and consequences of pioneer factor binding to nucleosomes. *Current opinion in structural biology* **2022**, *75*, 102425.

(17) Morgunova, E.; Taipale, J. Structural insights into the interaction between transcription factors and the nucleosome. *Current Opinion in Structural Biology* **2021**, *71*, 171–179.

(18) Jenuwein, T.; Allis, C. D. Translating the histone code. *Science* **2001**, *293*, 1074–1080.

(19) Weidemüller, P.; Kholmatov, M.; Petsalaki, E.; Zaugg, J. B. Transcription factors: Bridge between cell signaling and gene regulation. *Proteomics* **2021**, *21*, 2000034.

(20) Mariño Ramírez, L.; Kann, M. G.; Shoemaker, B. A.; Landsman, D. Histone structure and nucleosome stability. *Expert Rev Proteomics* **2005**, *2*, 719–729.

(21) Wood, C. M.; Nicholson, J. M.; Lambert, S. J.; Chantalat, L.; Reynolds, C. D.; Baldwin, J. P. High-resolution structure of the native histone octamer. *Acta Crystallogr Sect F Struct Biol Cryst Commun* **2005**, *61*, 541–545.

(22) Cutter, A. R.; Hayes, J. J. A brief review of nucleosome structure. *FEBS Lett* **2015**, *589*, 2914–2922.

(23) Pennings, S.; Allan, J.; Davey, C. S. DNA methylation, nucleosome formation and positioning. *Briefings in Functional Genomics* **2005**, *3*, 351–361.

(24) McGinty, R. K.; Tan, S. Nucleosome structure and function. *Chemical reviews* **2015**, *115*, 2255–2273.

(25) Ghoneim, M.; Fuchs, H. A.; Musselman, C. A. Histone tail conformations: a fuzzy affair with DNA. *Trends in biochemical sciences* **2021**, *46*, 564–578.

(26) Peng, Y.; Li, S.; Onufriev, A.; Landsman, D.; Panchenko, A. R. Binding of regulatory proteins to nucleosomes is modulated by dynamic histone tails. *Nature communications* **2021**, *12*, 5280.

(27) Peng, Y.; Li, S.; Landsman, D.; Panchenko, A. R. Histone tails as signaling antennas of chromatin. *Current opinion in structural biology* **2021**, *67*, 153–160.

(28) Prakash, K.; Fournier, D. Evidence for the implication of the histone code in building the genome structure. *Biosystems* **2018**, *164*, 49–59.

(29) Fenley, A. T.; Anandakrishnan, R.; Kidane, Y. H.; Onufriev, A. V. Modulation of nucleosomal DNA accessibility via charge-altering post-translational modifications in histone core. *Epigenetics & chromatin* **2018**, *11*, 1–19.

(30) Morrison, E. A.; Bowerman, S.; Sylvers, K. L.; Wereszczynski, J.; Musselman, C. A. The conformation of the histone H3 tail inhibits association of the BPTF PHD finger with the nucleosome. *Elife* **2018**, *7*.

(31) Morrison, E. A.; Baweja, L.; Poirier, M. G.; Wereszczynski, J.; Musselman, C. A. Nucleosome composition regulates the histone H3 tail conformational ensemble and accessibility. *Nucleic acids research* **2021**, *49*, 4750–4767.

(32) Tsunaka, Y.; Furukawa, A.; Nishimura, Y. Histone tail network and modulation in a nucleosome. *Current Opinion in Structural Biology* **2022**, *75*, 102436.

(33) Li, H.; Ilin, S.; Wang, W.; Duncan, E. M.; Wysocka, J.; Allis, C. D.; Patel, D. J. Molecular basis for site-specific read-out of histone H3K4me3 by the BPTF PHD finger of NURF. *Nature* **2006**, *442*, 91–95.

(34) He, C.; Liu, N.; Xie, D.; Liu, Y.; Xiao, Y.; Li, F. Structural basis for histone H3K4me3 recognition by the N-terminal domain of the PHD finger protein Spp1. *Biochemical Journal* **2019**, *476*, 1957–1973.

(35) Sanchez, R.; Zhou, M. M. The PHD finger: a versatile epigenome reader. *Trends Biochem Sci* **2011**, *36*, 364–372.

(36) Jain, K.; Fraser, C. S.; Marunde, M. R.; Parker, M. M.; Sagum, C.; Burg, J. M.; Hall, N.; Popova, I. K.; Rodriguez, K. L.; Vaidya, A., et al. Characterization of the plant homeodomain (PHD) reader family for their histone tail interactions. *Epigenetics & chromatin* **2020**, *13*, 1–11.

(37) Fujisawa, T.; Filippakopoulos, P. Functions of bromodomain-containing proteins and their roles in homeostasis and cancer. *Nature Reviews Molecular Cell Biology* **2017**, *18*, 246–262.

(38) Zaware, N.; Zhou, M.-M. Bromodomain biology and drug discovery. *Nat. Struct. Mol. Biol.* **2019**, *26*, 870–879.

(39) Zahid, H.; Olson, N. M.; Pomerantz, W. C. K. Opportunity knocks for uncovering the new function of an understudied nucleosome remodeling complex member, the bromodomain PHD finger transcription factor, BPTF. *Curr. Opin. Struct. Biol.* **2021**, *63*, 57–67.

(40) Schneider, R.; Bannister, A. J.; Myers, F. A.; Thorne, A. W.; Crane-Robinson, C.; Kouzarides, T. Histone H3 lysine 4 methylation patterns in higher eukaryotic genes. *Nat. Cell Biol.* **2004**, *6*, 73–77.

(41) Bernstein, B. E.; Kamal, M.; Lindblad-Toh, K.; Bekiranov, S.; Bailey, D. K.; Huebert, D. J.; McMahon, S.; Karlsson, E. K.; Kulbokas III, E. J.; Gingeras, T. R.; Schreiber, S. L.; Lander, E. S. Genomic Maps and Comparative Analysis of Histone Modifications in Human and Mouse. *Cell* **2005**, *120*, 169–181.

(42) Wysocka, J.; Swigut, T.; Milne, T. A.; Dou, Y.; Zhang, X.; Burlingame, A. L.; Roeder, R. G.; Brivanlou, A. H.; Allis, C. D. WDR5 Associates with Histone H3 Methylated at K4 and Is Essential for H3 K4 Methylation and Vertebrate Development. *Cell* **2005**, *121*, 859–872.

(43) Barak, O.; Lazzaro, M. A.; Lane, W. S.; Speicher, D. W.; Picketts, D. J.; Shiekhattar, R. Isolation of human NURF: a regulator of Engrailed gene expression. *The EMBO journal* **2003**, *22*, 6089–6100.

(44) Mariani, L.; Lussi, Y. C.; Vandamme, J.; Riveiro, A.; Salcini, A. E. The H3K4me3/2 histone demethylase RBR-2 controls axon guidance by repressing the actin-remodeling gene wsp-1. *Development* **2016**, *143*, 851–863.

(45) Alkhatib, S. G.; Landry, J. W. The Nucleosome Remodeling Factor. *FEBS Lett.* **2011**, *585*, 3197–3207.

(46) Hamiche, A.; Kang, J.-G.; Dennis, C.; Xiao, H.; Wu, C. Histone tails modulate nucleosome mobility and regulate ATP-dependent nucleosome sliding by NURF. *Proceedings of the National Academy of Sciences* **2001**, *98*, 14316–14321.

(47) Bezrookove, V.; Khan, I. A.; Nosrati, M.; Miller III, J. R.; McAllister, S.; Dar, A. A.; Kashani-Sabet, M. BPTF promotes the progression of distinct subtypes of breast cancer and is a therapeutic target. *Frontiers in Oncology* **2022**, *12*, 1011173.

(48) Mélin, L.; Calosing, C.; Kharenko, O. A.; Hansen, H. C.; Gagnon, A. Synthesis of NVS-BPTF-1 and evaluation of its biological activity. *Bioorganic & Medicinal Chemistry Letters* **2021**, *47*, 128208.

(49) Dai, M.; Lu, J.-J.; Guo, W.; Yu, W.; Wang, Q.; Tang, R.; Tang, Z.; Xiao, Y.; Li, Z.; Sun, W., et al. BPTF promotes tumor growth and predicts poor prognosis in lung adenocarcinomas. *Oncotarget* **2015**, *6*, 33878.

(50) Song, J.-J.; Garlick, J. D.; Kingston, R. E. Structural basis of histone H4 recognition by p55. *Genes & development* **2008**, *22*, 1313–1318.

(51) McGinty, R. K.; Makde, R. D.; Tan, S. *Methods in enzymology*; 2016; Vol. 573; pp 43–65.

(52) Woods, D. C.; Wereszczynski, J. Elucidating the influence of linker histone variants on chromatosome dynamics and energetics. *Nucleic acids research* **2020**, *48*, 3591–3604.

(53) Armeev, G. A.; Kniazeva, A. S.; Komarova, G. A.; Kirpichnikov, M. P.; Shaytan, A. K. Histone dynamics mediate DNA unwrapping and sliding in nucleosomes. *Nature communications* **2021**, *12*, 2387.

(54) Peng, Y.; Li, S.; Onufriev, A.; Landsman, D.; Panchenko, A. R. Binding of regulatory proteins to nucleosomes is modulated by dynamic histone tails. *Nat. Commun.* **2021**, *12*.

(55) Portillo-Ledesma, S.; Li, Z.; Schlick, T. Genome modeling: from chromatin fibers to genes. *Current opinion in structural biology* **2023**, *78*, 102506.

(56) Khatua, P.; Tang, P.; Moulick, A. G.; Patel, R.; Manandhar, A.; Loverde, S. M. Sequence dependence in nucleosome dynamics. *Biophysical Journal* **2024**, *123*, 137a.

(57) Fedulova, A. S.; Armeev, G. A.; Romanova, T. A.; Singh-Palchevskaia, L.; Kosarim, N. A.; Motorin, N. A.; Komarova, G. A.; Shaytan, A. K. Molecular dynamics simulations of nucleosomes are coming of age. *Wiley Interdisciplinary Reviews: Computational Molecular Science* **2024**, *14*, e1728.

(58) Sali, A.; Blundell, T. L. Comparative protein modelling by satisfaction of spatial restraints. *J Mol Biol* **1993**, *234*, 779–815.

(59) Pettersen, E. F.; Goddard, T. D.; Huang, C. C.; Couch, G. S.; Greenblatt, D. M.; Meng, E. C.; Ferrin, T. E. UCSF Chimera—a visualization system for exploratory research and analysis. *J. Comput. Chem.* **2004**, *25*, 1605–1612.

(60) Case, D. A. et al. AMBER 20. *University of California, San Francisco* **2020**,

(61) Tian, C.; Kasavajhala, K.; Belfon, K. A. A.; Raguette, L.; Huang, H.; Migues, A. N.; Bickel, J.; Wang, Y.; Pincay, J.; Wu, Q.; Simmerling, C. ff19SB: Amino-Acid-Specific Protein Backbone Parameters Trained against Quantum Mechanics Energy Surfaces in Solution. *J. Chem. Theory Comput.* **2020**, *16*, 528–552.

(62) Papamokos, G. V.; Tziatzos, G.; Papageorgiou, D. G.; Georgatos, S. D.; Politou, A. S.; Kaxiras, E. Structural role of RKS motifs in chromatin interactions: a molecular dy-

namics study of HP1 bound to a variably modified histone tail. *Biophysical journal* **2012**, *102*, 1926–1933.

(63) Izadi, S.; Anandakrishnan, R.; Onufriev, A. V. Building Water Models: A Different Approach. *J. Phys. Chem. Lett.* **2014**, *5*, 3863–3871.

(64) Sengupta, A.; Li, Z.; Song, L. F.; Li, P.; Merz, K. M. J. Parameterization of monovalent ions for the OPC3, OPC, TIP3P-FB, and TIP4P-FB water models. *J. Chem. Inf. Model.* **2021**, *61*, 869–880.

(65) Li, P.; Song, L. F.; Merz, K. M. J. Systematic parameterization of monovalent ions employing the nonbonded model. *J. Chem. Theory Comput.* **2015**, *11*, 1645–1657.

(66) Ivani, I. et al. Parmbsc1: A refined force field for DNA simulations. *Nat. Methods* **2016**, *13*, 55–58.

(67) Peters, M. B.; Yang, Y.; Wang, B.; Füsti-Molnár, L.; Weaver, M. N.; Merz, K. M. J. Structural Survey of Zinc-Containing Proteins and Development of the Zinc AMBER Force Field (ZAFF). *J. Chem. Theory Comput.* **2010**, *6*, 2935–2947.

(68) Hopkins, C. W.; Le Grand, S.; Walker, R. C.; Roitberg, A. E. Long-Time-Step Molecular Dynamics through Hydrogen Mass Repartitioning. *J. Chem. Theory Comput.* **2015**, *11*, 1864–1874.

(69) Berendsen, H. J.; Postma, J. v.; Van Gunsteren, W. F.; DiNola, A.; Haak, J. R. Molecular dynamics with coupling to an external bath. *The Journal of chemical physics* **1984**, *81*, 3684–3690.

(70) Paquet, E.; Viktor, H. L. Molecular dynamics, monte carlo simulations, and langevin dynamics: a computational review. *BioMed research international* **2015**, *2015*, 183918.

(71) Gotz, A. W.; Williamson, M. J.; Xu, D.; Poole, D.; Le Grand, S.; Walker, R. C. Routine microsecond molecular dynamics simulations with AMBER on GPUs. 1. Generalized born. *Journal of chemical theory and computation* **2012**, *8*, 1542–1555.

(72) Salomon-Ferrer, R.; Gotz, A. W.; Poole, D.; Le Grand, S.; Walker, R. C. Routine microsecond molecular dynamics simulations with AMBER on GPUs. 2. Explicit solvent particle mesh Ewald. *Journal of chemical theory and computation* **2013**, *9*, 3878–3888.

(73) Le Grand, S.; Götz, A. W.; Walker, R. C. SPFP: Speed without compromise—A mixed precision model for GPU accelerated molecular dynamics simulations. *Computer Physics Communications* **2013**, *184*, 374–380.

(74) Towns, J.; Cockerill, T.; Dahan, M.; Foster, I.; Gaither, K.; Grimshaw, A.; Hazlewood, V.; Lathrop, S.; Lifka, D.; Peterson, G. D.; Roskies, R.; Scott, J. R.; Wilkins-Diehr, N. XSEDE: Accelerating Scientific Discovery. *Comput. Sci. Eng.* **2014**, *16*, 62–74.

(75) Humphrey, W.; Dalke, A.; Schulten, K. VMD – Visual Molecular Dynamics. *J. Mol. Graph.* **1996**, *14*, 33–38.

(76) Laurent, B.; Chavent, M.; Cragnolini, T.; Dahl, A. C. E.; Pasquali, S.; Derreumaux, P.; Sansom, M. S. P.; Baaden, M. Epock: Rapid analysis of protein pocket dynamics. *Bioinformatics* **2014**, *31*, 1478–1480.

(77) Tekpinar, M.; Neron, B.; Delarue, M. Extracting dynamical correlations and identifying key residues for allosteric communication in proteins by correlationplus. *J. Chem. Inf. Model.* **2021**, *61*, 4832–4838.

(78) Weiser, J.; Shenkin, P. S.; Still, W. C. Approximate atomic surfaces from linear combinations of pairwise overlaps (LCPO). *Journal of Computational Chemistry* **1999**, *20*, 217–230.

(79) Michaud-Agrawal, N.; Denning, E. J.; Woolf, T. B.; Beckstein, O. MDAnalysis: A toolkit for the analysis of molecular dynamics simulations. *Journal of Computational Chemistry* **2011**, *32*, 2319–2327.

(80) Richard J. Gowers,; Max Linke,; Jonathan Barnoud,; Tyler J. E. Reddy,; Manuel N. Melo,; Sean L. Seyler,; Jan Domański,; David L. Dotson,; Sébastien Buchoux,; Ian M. Kenney,; Oliver Beckstein, MDAnalysis: A Python Package for the Rapid Analysis of Molecular Dynamics Simulations. **2016**, 98 – 105.

(81) Chen, W.-h.; Fu, J. Y.; Kourentzi, K.; Willson, R. C. Nucleic acid affinity of clustered-charge anion exchange adsorbents: Effects of ionic strength and ligand density. *Journal of Chromatography A* **2011**, *1218*, 258–262.

(82) Wang, E.; Sun, H.; Wang, J.; Wang, Z.; Liu, H.; Zhang, J. Z. H.; Hou, T. End-Point Binding Free Energy Calculation with MM/PBSA and MM/GBSA: Strategies and Applications in Drug Design. *Chem. Rev.* **2019**, *119*, 9478–9508.

(83) Miller III, B. R.; McGee Jr, T. D.; Swails, J. M.; Homeyer, N.; Gohlke, H.; Roitberg, A. E. MMPBSA. py: an efficient program for end-state free energy calculations. *Journal of chemical theory and computation* **2012**, *8*, 3314–3321.

(84) Nguyen, H.; Roe, D. R.; Simmerling, C. Improved Generalized Born solvent model parameters for protein simulations. *Journal of Chemical Theory and Computation* **2013**, *9*, 2020–2034.

(85) Nguyen, H.; Perez, A.; Bermeo, S.; Simmerling, C. Refinement of generalized born implicit solvation parameters for nucleic acids and their complexes with proteins. *Journal of chemical theory and computation* **2015**, *11*, 3714–3728.

(86) Chodera, J. D.; Swope, W. C.; Pitera, J. W.; Seok, C.; Dill, K. A. Use of the weighted

histogram analysis method for the analysis of simulated and parallel tempering simulations. *Journal of Chemical Theory and Computation* **2007**, *3*, 26–41.

(87) Shirts, M. R.; Chodera, J. D. Statistically optimal analysis of samples from multiple equilibrium states. *The Journal of chemical physics* **2008**, *129*.

(88) Ragvin, A.; Valvatne, H.; Erdal, S.; Årskog, V.; Tufteland, K. R.; Breen, K.; Øyan, A. M.; Eberharter, A.; Gibson, T. J.; Becker, P. B.; Aasland, R. Nucleosome Binding by the Bromodomain and PHD Finger of the Transcriptional Cofactor p300. *J. Mol. Biol.* **2004**, *337*, 773–788.

(89) Musselman, C. A.; Kutateladze, T. G. Handpicking epigenetic marks with PHD fingers. *Nucleic acids research* **2011**, *39*, 9061–9071.

(90) Barak, O.; Lazzaro, M. A.; Lane, W. S.; Speicher, D. W.; Picketts, D. J.; Shiekhattar, R. Isolation of human NURF: a regulator of Engrailed gene expression. *EMBO J.* **2003**, *22*, 6089–6100.

(91) Wysocka, J.; Swigut, T.; Xiao, H.; Milne, T. A.; Kwon, S. Y.; Landry, J.; Kauer, M.; Tackett, A. J.; Chait, B. T.; Badenhorst, P.; Wu, C.; Allis, C. D. A PHD finger of NURF couples histone H3 lysine 4 trimethylation with chromatin remodelling. *Nature* **2006**, *442*, 86–90.

(92) Jordan-Sciutto, K. L.; Dragich, J. M.; Caltagarone, J.; Hall, D. J.; Bowser, R. Fetal Alz-50 Clone 1 (FAC1) Protein Interacts with the Myc-Associated Zinc Finger Protein (ZF87/MAZ) and Alters Its Transcriptional Activity. *Biochemistry* **2000**, *39*, 3206–3215.

(93) Oppikofer, M.; Bai, T.; Gan, Y.; Haley, B.; Liu, P.; Sandoval, W.; Ciferri, C.; Cochran, A. G. Expansion of the ISWI chromatin remodeler family with new active complexes. *EMBO Rep.* **2017**, *18*, 1697–1706.

(94) Morioka, S.; Sato, S.; Horikoshi, N.; Kujirai, T.; Tomita, T.; Baba, Y.; Kakuta, T.; Ogoshi, T.; Puppulin, L.; Sumino, A.; Umeda, K.; Kodera, N.; Kurumizaka, H.; Shibata, M. High-Speed Atomic Force Microscopy Reveals Spontaneous Nucleosome Sliding of H2A.Z at the Subsecond Time Scale. *Nano Lett.* **2023**, *23*, 1696–1704.

(95) Niina, T.; Brandani, G. B.; Tan, C.; Takada, S. Sequence-dependent nucleosome sliding in rotation-coupled and uncoupled modes revealed by molecular simulations. *PLoS Comput. Biol.* **2017**, *13*, 1–22.

(96) Schwammle, V.; Aspalter, C.-M.; Sidoli, S.; Jensen, O. N. Large scale analysis of co-existing post-translational modifications in histone tails reveals global fine structure of cross-talk. *Mol. Cell. Proteomics* **2014**, *13*, 1855–1865.